In-Air Rangefinding with an AlN Piezoelectric Micromachined Ultrasound Transducer

Richard J. Przybyla, *Student Member, IEEE*, Stefon E. Shelton, *Student Member, IEEE*, André Guedes, Igor I. Izyumin, *Student Member, IEEE*, Mitchell H. Kline, *Student Member, IEEE*, David A. Horsley, *Member, IEEE*, Bernhard E. Boser, *Fellow, IEEE*

***Abstract*—An ultrasonic rangefinder has a working range of 30 mm to 450 mm and operates at a 375 Hz maximum sampling rate. The random noise increases with distance and equals 1.3 mm at the maximum range. The range measurement principle is based on pulse-echo time-of-flight measurement using a single transducer for transmit and receive. The transducer consists of a piezoelectric AlN membrane with 400 μm diameter, which was fabricated using a low-temperature process compatible with processed CMOS wafers. The performance of the system exceeds the performance of other micromechanical rangefinders.**

I. Introduction

ULTRASONIC transducers have many applications including imaging, rangefinding for computer vision, human machine interaction, short-range navigation, nondestructive testing, and flow sensing. Ultrasonic rangefinding is an attractive alternative to radio frequency- and light-based rangers at short ($<$10 m) distances since the relatively low speed of sound alleviates the high speed electronics requirements of optical and RF solutions.

However, commercially available bulk piezoelectric transducers suffer from a poor acoustic impedance match to air, which results in poor transduction efficiency between the electrical and acoustical domains. The addition of special materials to the transducer surface can improve the efficiency, but only in a limited bandwidth [1]. Despite these shortcomings, rangefinders based on bulk transducers can achieve larger maximum ranges [2] than rangefinders based on micromachined transducers because their size translates into much higher output power. However, because of their size and power consumption, systems based on bulk transducers are not practical in mobile applications.

In the past fifteen years, the introduction of capacitive micromachined ultrasound transducers (cMUTs) [3]–[5] has reduced the power consumption and enabled two-dimensional arrays by miniaturizing the transducer using integrated circuit fabrication technology. Since the cMUT output pressure depends quadratically on the excitation voltage and the inverse of the capacitor gap, cMUT designs usually have submicron gaps [6] resulting in complex fabrication. The small gap translates into a small linear displacement range; this is especially significant in air-coupled transducers since the acoustic impedance of air is three orders of magnitude lower than that of water, limiting the output power for a given displacement. To partially overcome this, some air-coupled capacitive transducers use bias voltages of hundreds of volts [5], further increasing system complexity.

Piezoelectric micromachined ultrasound transducers (pMUTs) [7], [8] do not require high voltage. The pMUT's linear displacement range is a function of the membrane thickness [9], which can be increased at the cost of only a linear reduction in the electromechanical coupling factor. In addition, the aluminum nitride (AlN) piezoelectric layer used in this work [10] is readily integrable with foundry CMOS, enabling fully integrated solutions with on-chip signal processing. This is particularly attractive in applications requiring multiple transducers for beam forming and imaging.

Aluminum nitride is also attractive for rangefinding. AlN has a higher piezoelectric coefficient than ZnO, resulting in increased output power and receive sensitivity. AlN's piezoelectric coefficient is one-tenth that of PZT, but AlN's dielectric constant is less than one-hundredth that of PZT. This results in an improvement in the signal to noise ratio in designs that use AlN compared to those that use PZT, due to the lower parallel plate capacitance.

Ultrasonic rangefinders operate either in continuous wave (CW) mode or pulse-echo (PE) mode. Narrowband CW systems suffer from multipath fading that can cause large range errors [11]. Frequency modulated continuous wave (FMCW) excitation can overcome multipath fading [12], but requires very high dynamic range since the transmitted signal dwarfs the return signal. PE excitation has lower average output power compared to CW, but the transmit pulse and return echoes are separated in time. This avoids the dynamic range and multipath problems that plague CW systems.

The performance of a rangefinding system depends on the output power and operating frequency. Bulk transducer based systems [2] can achieve large ($>$10 m) maximum range [13] or millimeter accuracy [14]. Micromachined transducer based systems suffer from lower output power because of the small actuation area. A system that used a thermally actuated micromachined transducer [11] demonstrated millimeter accuracy and 11 cm range. Hybrid systems, which

Manuscript received February 1, 2011, revised May 15, 2011.

An earlier version of this paper was presented at the 2010 IEEE SENSORS Conference and was published in its proceedings.

This material is based upon work supported by the Defense Advanced Research Projects Agency (DARPA) and/or the Space and Naval Warfare Center, San Diego (SPAWAR SSC-SD) under Contract No. N66001-08-C-2023

R. Przybyla, I. Izyumin, M. Kline, and B. Boser are with the Berkeley Sensor and Actuator Center, University of California, Berkeley, CA 94720 (e-mail: rjp@berkeley.edu).

S. Shelton, A. Guedes, and D. Horsley are with the Berkeley Sensor and Actuator Center, University of California, Davis, CA 95616.

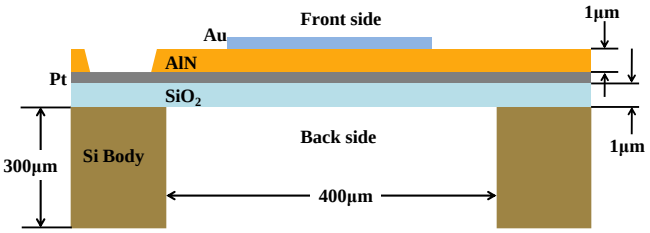

Fig. 1. Cross-section of piezoelectric micromachined ultrasound transducer.

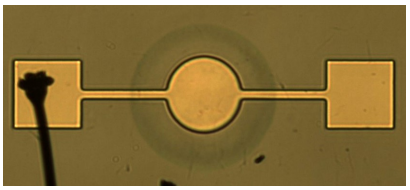

Fig. 2. Optical micrograph of pMUT.

use a bulk transmitter and a micromachined receiver, can achieve millimeter accuracy and >70 cm range [15] due to the increased output power.

This paper expands on the work presented in [16]. In Section II we present a model for the pMUT and the acoustic channel which includes electrical, mechanical, and acoustic domains. The model is the basis for a pulse-echo ultrasonic rangefinder based on a single pMUT, which is presented in Section III. The device operates over a working range of 30 mm - 450 mm. The measurement error consists of a random component dominated by noise sources in the transducer and a systematic error caused by the range ambiguity that results from the divergence of the beam and a systematic error caused by the demodulation technique. The random error increases with distance and is 1.3 mm at 450 mm.

II. Theory and Characterization Data

A. Device Structure

The ultrasound transducer [10] consists of a circular unimorph membrane with diameter 400 μm consisting of an SiO_2/Pt/AlN/Au sandwich fabricated on a Si wafer. As Fig. 1 shows, a hole etched though the wafer exposes both sides of the membrane. The electrical field resulting from a voltage applied between the Au and Pt electrodes results in a transverse stress in the AlN layer and consequent out-of-plane bending of the membrane, which produces a pressure wave. Similarly, an incident pressure wave results in membrane deformation and consequent charge on the electrodes, enabling the device to be used both as a transmitter and receiver. For optimum pMUT performance the top electrode should cover the area of the membrane where its displacement curve has positive curvature. For this pMUT the optimum electrode/membrane diameter ratio size was found to be 70%, resulting in an electrode diameter of 275μm. No dc bias is required for device operation, but the device can be tuned using a dc bias. The transducer's resonant frequency has a dc bias sensitivity of 800Hz/V. Fig. 2 shows an optical micrograph of the pMUT.

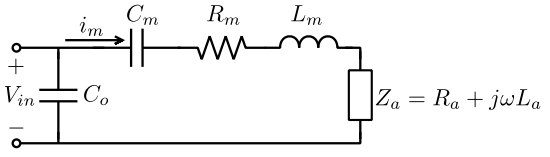

Fig. 3. Electrical model of transducer.

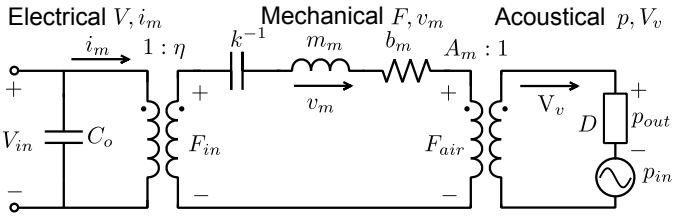

Fig. 4. Electrical, mechanical, and acoustical model of ultrasound transducer.

TABLE I
Values of Various Parameters at Resonance

Description	Electrical	Mechanical	Acoustical
Stiffness	C_m : 82.3 fF	k : 500 N/m	—
Membrane mass	L_m : 6.1 H	m_m : 250 ng	—
Acoustic mass	L_a : 0.62 H	m_a : 25 ng	ρ_A : 660 $\frac{\mu g}{mm^2}$
Substrate damping	R_m : 385 kΩ	b_m : 16 $\frac{\mu Ns}{m}$	—
Air damping	R_a : 69 kΩ	b_a : 2.8 $\frac{\mu Ns}{m}$	$\mathrm{Re}(D)$: 2 $\frac{kRayls}{mm^2}$
Coupling ratio	—	η : 6.4 $\frac{\mu N}{V}$	A_m : 0.038 mm^2
Feedthrough	C_o : 14.6 pF	—	—
Resonant frequency	f_o : 214 kHz		
Quality factor	Q : 20		

Since the pMUT diameter/thickness ratio is very high, the residual stress plays an important role in the device performance. The pMUT displacement and resonance frequency are strongly dependent on the overall membrane residual stress. For that reason, the deposition of the membrane layers (SiO_2/AlN) was tuned so that the overall stress was close to zero. Another effect that can cause variations is surface roughness of the SiO_2 layer, which influences the quality of the piezoelectric AlN layer, and hence the device performance. To minimize oxide roughness, chemical–mechanical polishing was performed after oxide deposition. The backside etch stops on the SiO_2 layer, so over–etch could also cause some variation in the displacement and resonant frequency of the device.

B. Transducer Electromechanical Model

For small displacements (<0.4 μm) the membrane behaves like a linear resonator. Fig. 3 shows an electrical equivalent circuit. In this model, capacitor C_m models the equivalent lumped membrane stiffness, inductor L_m models the mass, and resistor R_m models the loss to the substrate. Impedance Z_a represents the interface to the air. The resistive part R_a models the acoustic power delivered to or received from the air. The values of C_o, C_m, $R_p = R_m + R_a$, and $L_p = L_m + L_a$, as well as the resonant frequency f_o and the quality factor Q

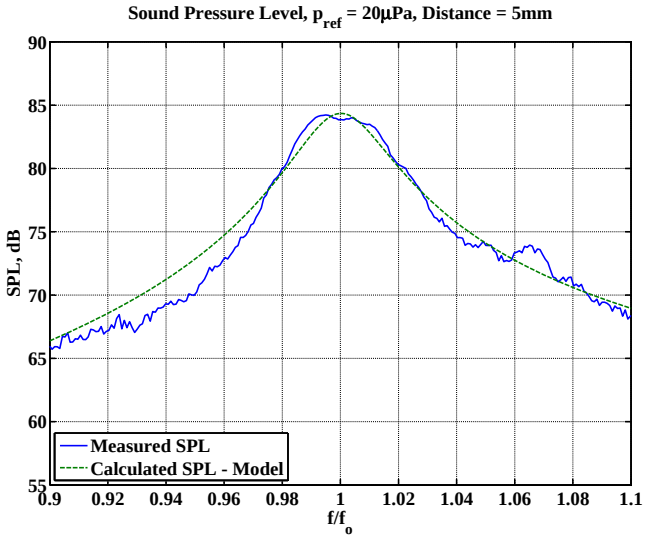

Fig. 5. SPL vs. normalized frequency from measurement and theory.

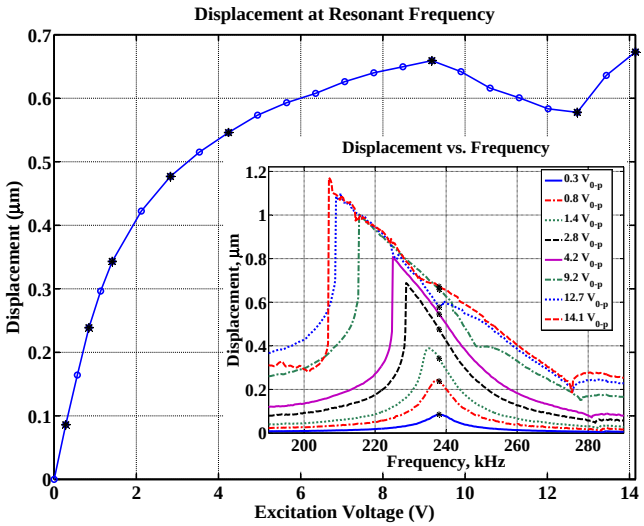

Fig. 6. Membrane displacement as a function of drive voltage amplitude V_{in} at the linear resonant frequency. The inset shows the membrane displacement vs. frequency for different drive voltages. The dip at high drive amplitude is due to an undesirable mode that shifts into the measurement band.

can be measured with a network analyzer and are listed in Table I.

The electrical model accurately reflects the characteristics of the transducer at its electrical port, but only indirectly describes its mechanical and acoustic properties. Fig. 4 shows a refined model where all domains are represented explicitly and coupled with ideal transformers. In this model all components are represented by electrical equivalents. In the mechanical domain, voltage and current correspond to force and membrane velocity v_m. In the acoustic domain, voltage and current correspond to pressure and volume velocity $\mathrm{V}_v = v_m A_m$, respectively, where A_m is the effective area of the membrane.

The coupling coefficient $\eta = F_{in}/V_{in}$ between the electrical and mechanical domains can be determined from a measurement of the membrane displacement at resonance, $x(\omega_o)$ using a laser Doppler vibrometer (LDV). At resonance, the voltage across capacitor C_m equals QV_{in}, and the force on the spring k is $kx(\omega_o)$, thus $\eta Q V_{in} = kx(\omega_o)$. Using $k = \eta^2/C_m$ yields

$$\eta = \frac{QV_{in}C_m}{x(\omega_o)}. \tag{1}$$

The mechanical force on the air, F_{air}, establishes a pressure difference $p_{air} = F_{air}/A_m$ between the front- and back side of the membrane. In the model, D represents the acoustic impedance of the air, $D = p_{air}/V_v$, and is given by [17]

$$D = \frac{\rho c}{A_m}\left(1 - \frac{2J_1(2wa)}{2wa} + j\frac{2K_1(2wa)}{2wa}\right), w = \frac{2\pi}{\lambda} \tag{2}$$

In this equation, ρ is the density of air, $\lambda \approx 1.6\,\mathrm{mm}$ is the wavelength of sound at f_o, J_1 is the first order Bessel function, K_1 is the first order Struve function, and a is the effective radius of the membrane. The real part of (2) models real power delivered to the air, and the electrical equivalent is

$$R_a = \mathrm{Re}(D)\frac{A_m^2}{\eta^2} \tag{3}$$

Maximum power transfer to the air is achieved when the resistance of the air R_a is equal to the mechanical loss R_m. Since the membrane radius is smaller than the wavelength, the real part of (2) is approximately 0.2, resulting in a lower than optimal value for R_a. Although this decreases the mechanical efficiency to 15%, the transduction efficiency of the device is still significantly higher than that of bulk devices [1]. The 2μm thick membrane The mechanical efficiency could be increased with a design that uses a partially released membrane to reduce anchor losses. Table I summarizes the measured device parameters. The conversion factor at resonance is $s_{out} = p_{out}/V_{in}$ =26 Pa/V and short-circuit current sensitivity is $s_i = i_m/p_{in}$ =13 nA/Pa.

C. Return Echo Attenuation

In a rangefinder, the echo signal strength depends on the target distance and acoustic reflectivity. The latter is near unity since the acoustic impedance of most materials is several orders of magnitude larger than that of air. Since $\lambda \gg a$ at resonance for the pMUT, the acoustic energy radiates isotropically from the front side of the transducer, resulting in a linear attenuation of pressure with distance. Additionally, the vibration of the air molecules give rise to an exponential loss [18]. Assuming a large target with perfect reflectivity, the ratio of the received to the transmitted pressure is

$$G_{ch} = \frac{p_{in}}{p_o} = \underbrace{\frac{a}{4R_T}}_{\text{spreading}} \underbrace{10^{-2\alpha R_T}}_{\text{loss}}, \tag{4}$$

where R_T is the range to the target, $\alpha = 3.61\times10^{-6} f - 0.0985$ is the attenuation constant in bels/meter, and f is the frequency of the sound wave. The vibration loss constant α increases with increasing humidity; the worst–case value is given here. For example, at $R_T = 400\,\mathrm{mm}$ and $f = 200\,\mathrm{kHz}$, the attenuation is $p_{in}/p_o = -93\,\mathrm{dB}$. The spreading term dominates up to approximately 1m. At 400 mm, the loss term contributes $-10\,\mathrm{dB}$.

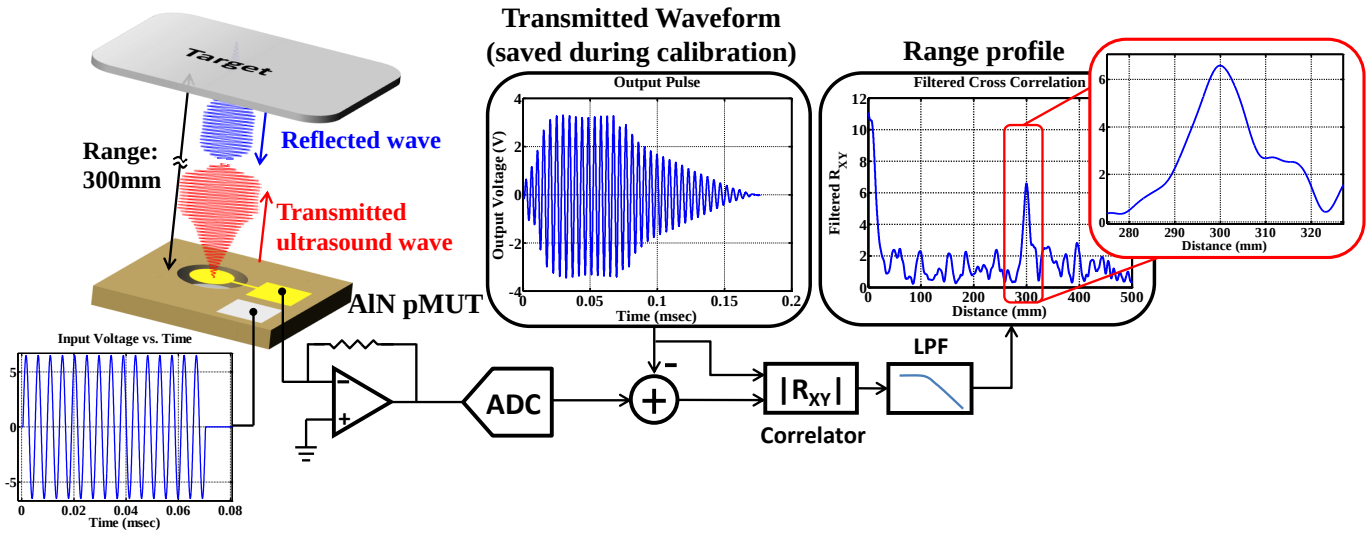

Fig. 7. Block diagram of rangefinder.

Because of the funnel created by the through-wafer hole below the membrane, the back side of the transducer is most sensitive in the direction normal to the membrane. As a result, round-trip attenuation in this direction is less than predicted by the equation stated above. The measured improvement is 17.1 dB, and the measured full–width half–maximum beam width is approximately 40°. In rangefinder applications the narrower radiation pattern from the backside has two advantages. The larger return signal improves the signal-to-noise ratio and hence the maximum range of the system. In addition, the better focus reduces the error caused by target range ambiguity.

D. Model Verification with Acoustic Test

To verify the model, the pMUT was driven near resonance with $V_{in} = 400\,\mathrm{mV}_{rms}$ and the acoustic output was measured with a high frequency microphone mounted 5 mm from the front surface of the pMUT. Fig. 5 compares the measured sound pressure level (SPL) to the prediction from the model and shows excellent agreement.

E. Nonlinearity

The transducer has significant nonlinearity at high displacement amplitudes. As Fig. 6 shows, the maximum amplitude at the linear resonant frequency is limited to less than 0.7 μm. The inset of Fig. 6 shows that when the excitation voltage is increased above 9V, an extraneous mode shifts into the measurement band and causes a dip in the displacement amplitude.

III. Rangefinder

A. System Overview

The transducer described above is used in the acoustic pulse-echo rangefinder shown conceptually in Fig. 7. The pMUT is excited with a burst at its resonant frequency f_o resulting in an acoustic wave being emitted and subsequently reflected by the target. The backside of the transducer is used to realize the benefits discussed above.

A transimpedance amplifier measures current (which is proportional to the membrane velocity) resulting from the acoustic echo. The target distance R_T is then calculated from the delay $\tau = 2R_T/c$ and the speed of sound, c.

A single transducer is used to transmit the burst and receive the echo. Using separate transmitter and receiver elements would decrease the minimum range and could potentially allow separate pMUT designs optimized for transmit or receive. However, matching between devices is both critical and difficult since the Q of the transducers is 20 and residual stress prevents precise control of the resonant frequency.

B. Transmit Burst

The ideal implementation would use short, high power pulses with a well defined start to measure range; however, this goal is obstructed by the transducer's narrowband response and nonlinearity at large displacements. When operated in the linear regime at the resonant frequency, the transducer requires $Q/f_o \approx 93\mu$sec to reach the maximum output power, as Fig. 8 illustrates. When the transducer is operated in the nonlinear regime, the output power shows significant compression, but nonlinear operation still yields a substantial increase in the output power.

The transducer exhibits spring softening, and as Fig. 6 shows, a substantial increase in the displacement can be realized by operating at the nonlinear resonant frequency. However, since the pMUT operates in the linear regime during the receive phase, the signal-to-noise ratio is maximized by operating at the linear resonant frequency.

Nonlinear excitation results in a distorted envelope as Fig. 9 shows. For small excitation voltages the envelope has an exponential shape as the linear model predicts; for larger excitation voltages the envelope reaches the maximum value

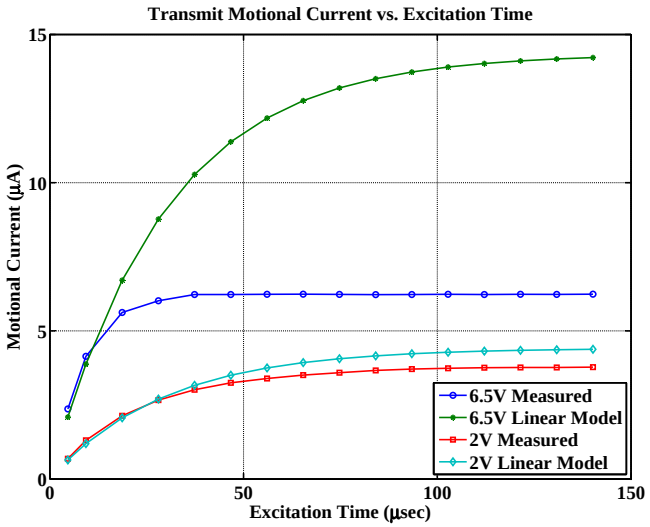

Fig. 8. Measured transmit motional current versus excitation time at resonance. As the comparison with the linear model shows, transducer nonlinearity reduces the time needed to reach peak output power but this comes at the cost of reduced output power.

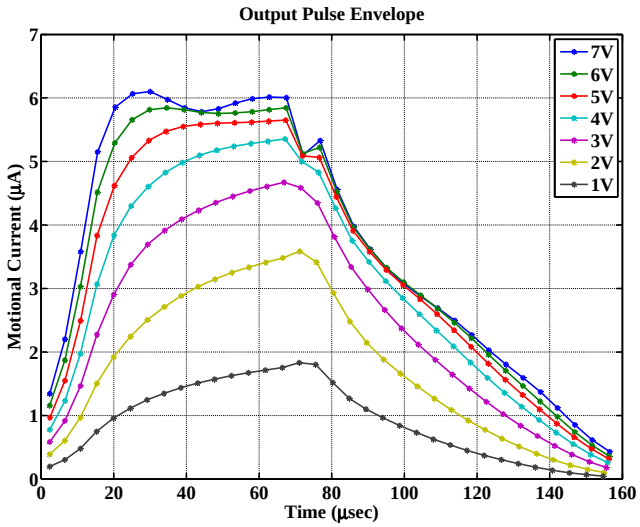

Fig. 9. Measured output pulse shape for different drive voltages when the device is excited at f_o for 70μsec.

much sooner, but the burst also decays more slowly. Fig. 10 shows that for large input voltages the settling time can be increased by nearly 20%, increasing the dead time in which no return echo can be received.

Excitation with amplitudes $\geq$7V causes the envelope to ring due to the second- and third- order spring coefficients, as Fig. 9 shows. This can cause errors in the measured range since the transmitted pulse is used as the search waveform for the matched filter. Because of this, the excitation amplitude was chosen to be 6.5V.

Using the transducer in the nonlinear regime requires that the transmit pulse decays and the system returns to the linear regime before the echo is received. The transmitted wave is shown in Fig. 7. At short range, the motional ring down current overlaps and corrupts the received echo, resulting in measurement errors. To suppress this error, the transmitted waveform is measured during a calibration phase and subsequently subtracted from the received signal.

The power required to drive the pMUT is dominated by $C_o V^2 f$ loss due to the parasitic capacitance of the device. For V_{exc} =6.5V, the excitation power is 575μW and the acoustic output power is 1.25μW; with an excitation time of 70μsec, the transmit energy consumption is only 40nJ per burst.

C. Receive Circuit

The round trip delay τ is determined from correlating the corrected return echo with the transmit pulse. The bandwidth of this matched filter is $B \approx f_o/N$, where N is the number of transmit cycles. Transmitting a longer pulse reduces the bandwidth and hence the noise at the output of the correlator. The resulting improved signal-to-noise ratio increases the maximum operating distance of the rangefinder as $\sqrt{N}$, neglecting loss, but the increased length of the pulse also increases the minimum operating range. The pulse must also be long enough to excite the narrowband response of the transducer when

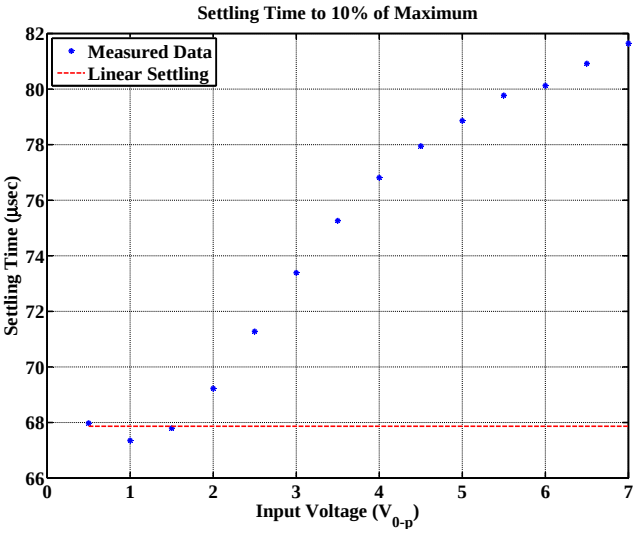

Fig. 10. Measured settling time to 10% of peak for different drive voltages with a 70μsec excitation at f_o.

it receives the echo. In this implementation, 15 cycles are transmitted at f_o resulting in a transmit time of 70μsec.

The periodicity of the transmit signal results in a $\pm\lambda/2$ periodicity of the correlation, resulting in a corresponding error in the range estimate, which is determined by taking the peak of the correlation vector. A linear averaging filter at the correlator output reduces the error. Due to this demodulation technique, there is a residual systematic error with period $\lambda/2$, which is shown in Fig. 11. The remaining error is dominated by thermal noise from the transducer and the interface circuits and has an approximately Gaussian distribution.

Fig. 7 shows a sample range profile for a target distance of R_T = 300 mm. The strong peak at zero range is due to imperfect cancellation of the transmit pulse and limits the minimum useful range to 30 mm.

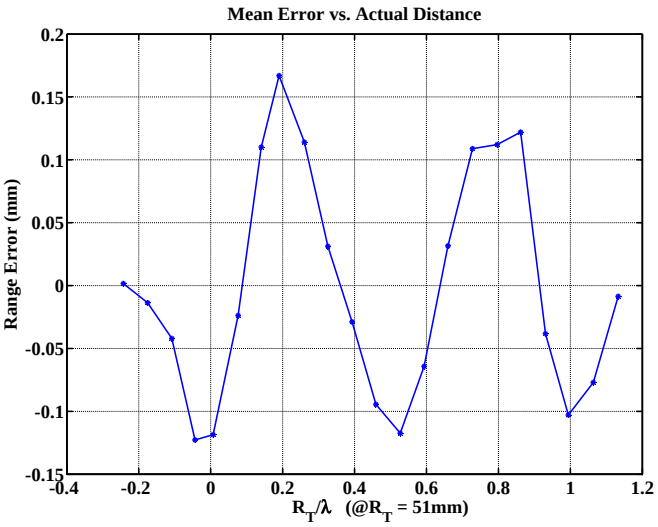

Fig. 11. Systematic error due to demodulation technique.

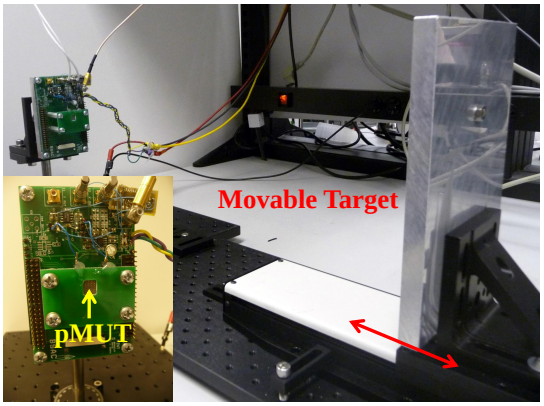

Fig. 12. Experimental setup. Inset shows prototype circuit board with pMUT mounted with backside facing target.

D. Results

The prototype rangefinder was tested using a moving stage with a metal target. Fig. 12 shows the experimental setup. The rangefinder has a working range of 30 mm to 450 mm. No averaging is used; the sample rate is limited to 375Hz by the round-trip delay of 2.6 ms at the maximum range at room temperature.

Fig. 13 shows the measured random noise as a function of target range. At short ranges, it increases linearly with distance due to increased signal attenuation as predicted by (4) in the regime where spreading dominates. At longer ranges, the increased attenuation results in increased distance noise. As Fig. 13 shows, the increase is approximately 7.8dB at 400mm, close to the theoretical result of 10dB predicted by (4). This discrepancy is likely explained by the fact that (4) uses the worst–case value for α, which occurs at maximum humidity. The dominant noise sources are the mechanical and acoustic damping in the transducer modeled by the Johnson noise from R_m and R_a in the transducer model, as well as noise from the transresistance amplifier. Lowering the parasitic capacitance C_o reduces the amplifier noise gain and hence its contribution

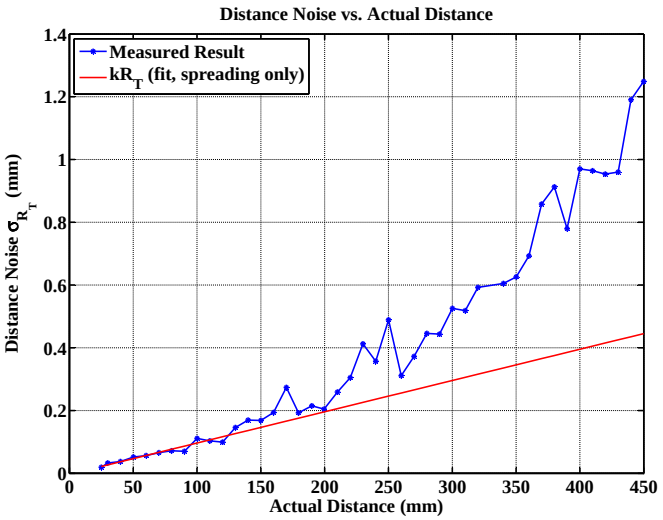

Fig. 13. Random distance noise versus target range R_T. Red line shows the short-range fit where the distance noise increases primarily due to spreading.

TABLE II
PERFORMANCE COMPARISON

Reference	Type	Max Range	Accuracy
[2]	Electrostatic	10 m [13]	25.4 mm [13]
[14]	Bulk	5 m	1 mm
[15]	Hybrid	>0.7 m	<4 mm
[11]	μmachined	0.11 m	4 mm
This work	μmachined	0.45 m	3.9 mm (3σ)

to the overall noise.

The temperature dependence of the speed of sound adds an additional error of 0.2 %/^{o}C. Its effect can be reduced with temperature compensation.

Table II shows a performance comparison to previous work. This work exceeds the performance demonstrated by the micromechanical rangefinder in [11]. At ranges of less than 220 mm, the 3σ accuracy of this sensor exceeds the reported accuracy of the bulk rangefinder in [14].

IV. CONCLUSION

Piezoelectric micromachined ultrasound transducers enable compact and low-power short-distance ranging with millimeter or better accuracy. Unlike capacitive transducers, no high-voltage bias is required; the unimorph design leads to a very simple manufacturing process. The thin membrane structure results in significantly improved coupling to air compared to published results fabricated with bulk PZT. The current design uses a single device to transmit and receive to alleviate problems with resonant frequency matching. As a result, the system requires calibration to resolve echoes during the ring down of the transducer. Active damping could obviate the need for calibration. Beam divergence, which causes range ambiguity, could be mitigated in future systems with electronic frequency matching and arrays of devices. The performance of the system exceeds that of other micromechanical rangefinders, and approaches the accuracy achieved by piezoceramic-based solutions.

ACKNOWLEDGMENT

The authors would like to thank S. Gambini and A. Flynn for helpful advice.

REFERENCES

[1] M. Haller and B. Khuri-Yakub, "1-3 composites for ultrasonic air transducers," in *Proc. IEEE Ultrasonics Symp. 1992*, vol. 2, Oct. 1992, pp. 937–939.

[2] C. Biber, S. Ellin, E. Shenk, and J. Stempeck, "The Polaroid ultrasonic ranging system," in *Audio Engineering Society Convention 67*, Oct. 1980.

[3] M. Haller and B. Khuri-Yakub, "A surface micromachined electrostatic ultrasonic air transducer," *IEEE Trans. Ultrason., Ferroelectr., Freq. Control*, vol. 43, no. 1, pp. 1–6, Jan. 1996.

[4] I. Ladabaum, X. Jin, H. Soh, A. Atalar, and B. Khuri-Yakub, "Surface micromachined capacitive ultrasonic transducers," *IEEE Trans. Ultrason., Ferroelectr., Freq. Control*, vol. 45, no. 3, pp. 678 –690, May 1998.

[5] I. Wygant, M. Kupnik, J. Windsor, W. Wright, M. Wochner, G. Yaralioglu, M. Hamilton, and B. Khuri-Yakub, "50 kHz capacitive micromachined ultrasonic transducers for generation of highly directional sound with parametric arrays," *IEEE Trans. Ultrason., Ferroelectr., Freq. Control*, vol. 56, no. 1, pp. 193–203, Jan. 2009.

[6] O. Oralkan, A. Ergun, J. Johnson, M. Karaman, U. Demirci, K. Kaviani, T. Lee, and B. Khuri-Yakub, "Capacitive micromachined ultrasonic transducers: next-generation arrays for acoustic imaging?" *IEEE Trans. Ultrason., Ferroelectr., Freq. Control*, vol. 49, no. 11, pp. 1596 –1610, Nov. 2002.

[7] J. Bernstein, S. Finberg, K. Houston, L. Niles, H. Chen, L. Cross, K. Li, and K. Udayakumar, "Micromachined high frequency ferroelectric sonar transducers," *IEEE Trans. Ultrason., Ferroelectr., Freq. Control*, vol. 44, no. 5, pp. 960–969, Sep. 1997.

[8] P. Muralt, N. Ledermann, J. Paborowski, A. Barzegar, S. Gentil, B. Belgacem, S. Petitgrand, A. Bosseboeuf, and N. Setter, "Piezoelectric micromachined ultrasonic transducers based on PZT thin films," *IEEE Trans. Ultrason., Ferroelectr., Freq. Control*, vol. 52, no. 12, pp. 2276 –2288, Dec. 2005.

[9] V. Kaajakari, T. Mattila, A. Oja, and H. Seppa, "Nonlinear limits for single-crystal silicon microresonators," *J. Microelectromech. Syst.*, vol. 13, no. 5, pp. 715 – 724, Oct. 2004.

[10] S. Shelton, M.-L. Chan, H. Park, D. Horsley, B. Boser, I. Izyumin, R. Przybyla, T. Frey, M. Judy, K. Nunan, F. Sammoura, and K. Yang, "CMOS-compatible AlN piezoelectric micromachined ultrasonic transducers," in *Proc. IEEE Ultrasonics Symp. 2009*, Oct. 2009, pp. 402 –405.

[11] C. Kuratli and Q. Huang, "A CMOS ultrasound range-finder microsystem," *IEEE J. Solid-State Circuits*, vol. 35, no. 12, pp. 2005 –2017, Dec. 2000.

[12] S. Roehr, P. Gulden, and M. Vossiek, "Precise distance and velocity measurement for real time locating in multipath environments using a frequency-modulated continuous-wave secondary radar approach," *IEEE Trans. Microw. Theory Tech.*, vol. 56, no. 10, pp. 2329 –2339, Oct. 2008.

[13] R. A. Jarvis, "A perspective on range finding techniques for computer vision," *IEEE Trans. Pattern Anal. Mach. Intell.*, vol. 5, no. 2, pp. 122–139, Mar. 1983.

[14] D. Webster, "A pulsed ultrasonic distance measurement system based upon phase digitizing," *IEEE Trans. Instrum. Meas.*, vol. 43, no. 4, pp. 578 –582, Aug. 1994.

[15] K. Yamashita, K. Iwahashi, Y. Ohmura, and M. Okuyama, "Ultrasonic position measurement using phased array microsensors with resonant frequency variation," in *Proc. TRANSDUCERS 2007*, Jun. 2007, pp. 1271–1274.

[16] R. Przybyla, S. Shelton, A. Guedes, I. Izyumin, M. Kline, D. Horsley, and B. Boser, "An ultrasonic rangefinder based on an AlN piezoelectric micromachined ultrasound transducer," in *Proc. IEEE Sensors 2010*, Nov. 2010, pp. 2417–2421.

[17] D. T. Blackstock, *Fundamentals of Physical Acoustics*. John Wiley & Sons, 2000.

[18] L. B. Evans and H. E. Bass, "Tables of absorption and velocity of sound in still air at 68F," Wyle Labratories, Tech. Rep. Report WR72-2., Jan. 1972.

Richard J. Przybyla (S'08) was born in San Jose, California, in 1986. He received the B.S. degree in electrical engineering from Oregon State University, Corvallis, Oregon, in 2008.

Since 2008, he has been with the Berkeley Sensor & Actuator Center at the University of California, Berkeley, CA, where he is pursuing his Ph.D. in electrical engineering. He has held positions at Hewlett-Packard, Oregon State University, and was a visiting researcher at the Technische Universität Kaiserslautern in Germany. His research interests include mixed-signal integrated circuits and microelectromechanical systems.

Stefon E. Shelton (S'09) was born in Santa Barbara, CA, in 1979. He received a B.S. in optical science and engineering from the University of California, Davis located in Davis, CA, in 2004.

Currently, he is a Graduate Student Researcher in the MEMS lab at University of California, Davis. His research focuses on the modeling and fabrication of piezoelectric micromachined transducers.

Mr. Shelton is a member of the IEEE Ultrasonics, Ferroelectrics, and Frequency Control Society.

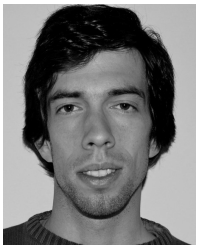

André Guedes received the M.S. and Ph.D. degrees in Physics Engineering from the Technical University of Lisbon, Portugal, in 2004 and 2010, respectively.

He is currently a post-doc researcher at University of Califonia, Davis and at the Berkeley Sensor & Actuator Center. His research interests include piezoelectric MEMS, ultrasonic devices, high-precision MEMS, and magnetic sensors.

Igor I. Izyumin (S'05) was born in Sevastopol, Ukraine, in 1985. He received B.S. degrees in electrical engineering and computer science from the University of Missouri, Rolla in 2008. He is currently pursuing the Ph.D. degree in electrical engineering at the University of California, Berkeley.

Between 2005 and 2006, he was with Adtran, Inc., Huntsville, AL, where he was involved with the development of mixed-signal ASICs. His research interests include MEMS sensor interfaces and mixed-signal integrated circuit design.

Mitchell H. Kline (S'06) was born in Temple, Texas on April 13, 1986. He received his B.S in computer engineering from Texas A&M University in College Station, Texas in 2008 and his M.S. in electrical engineering from the University of California, Berkeley in 2010. He is continuing to work toward his Ph.D. at Berkeley.

He interned at National Instruments in Austin, Texas in 2007 and Intrinsity in Bee Cave, Texas in 2008. His research interests include power electronics and analog integrated circuits.

David A. Horsley (M'97) received the B.S., M.S., and Ph.D. degrees in mechanical engineering at the University of California, Berkeley, CA, in 1992, 1994, and 1998, respectively.

He is an Associate Professor in the Department of Mechanical and Aerospace Engineering at the University of California, Davis, CA and has been a co-director of the Berkeley Sensor and Actuator Center (BSAC) since 2005. Prior to joining the faculty at UC Davis, Professor Horsley held research and development positions at Dicon Fiberoptics, Hewlett Packard Laboratories, and Onix Microsystems. His research interests include microfabricated sensors and actuators with applications in optical MEMS, communication, displays, and physical and biological sensors.

Dr. Horsley is a recipient of the NSF CAREER Award and the UC Davis College of Engineering's Outstanding Junior Faculty Award.

Bernhard E. Boser (F'03) received the Diploma in electrical engineering from the Swiss Federal Institute of Technology in 1984 and the M.S. and Ph.D. from Stanford University in 1985 and 1988.

From 1988 he was a Member of Technical Staff in the Adaptive Systems Department at AT&T Bell Laboratories. In 1992 he joined the faculty in the Department of Electrical Engineering and Computer Sciences at the University of California, Berkeley where he also serves as a Director of the Berkeley Sensor & Actuator Center. In 2004 he co-founded SiTime and in 2005/06 he was a visiting professor at the Institute of Micro- and Nanosystems at the Swiss Federal Institute of Technology in Zurich. His research is in the area of analog and mixed signal circuits, with special emphasis on analog-digital interface circuits and micromechanical sensors and actuators.

Dr. Boser has served on the program committees of the International Solid-State Circuits Conference, the Transducers Conference, the VLSI Symposium, and the Sensor and Actuator Workshop. He was the Editor of the IEEE JOURNAL OF SOLID-STATE CIRCUITS, served as the Chair of the Publications Committee, and is currently the President of the Solid-State Circuits Society. Dr. Boser is a Fellow of the IEEE and a distinguished lecturer of the SSCS.